NANO LETTERS

pubs.acs.org/NanoLett

Role of Kinetic Factors in Chemical Vapor Deposition Synthesis of Uniform Large Area Graphene Using Copper Catalyst

Sreekar Bhaviripudi,[†] Xiaoting Jia,[‡] Mildred S. Dresselhaus,[†,§] and Jing Kong*[,†]

[†]Department of Electrical Engineering and Computer Science, [‡]Department of Materials Science and Engineering, and [§]Department of Physics, Massachusetts Institute of Technology, Cambridge, Massachusetts 02139

ABSTRACT In this article, the role of kinetics, in particular, the pressure of the reaction chamber in the chemical vapor deposition (CVD) synthesis of graphene using low carbon solid solubility catalysts (Cu), on both the large area thickness uniformity and the defect density are presented. Although the thermodynamics of the synthesis system remains the same, based on whether the process is performed at atmospheric pressure (AP), low pressure (LP) (0.1−1 Torr) or under ultrahigh vacuum (UHV) conditions, the kinetics of the growth phenomenon are different, leading to a variation in the uniformity of the resulting graphene growth over large areas (wafer scale). The kinetic models for APCVD and LPCVD are discussed, thereby providing insight for understanding the differences between APCVD vs LPCVD/UHVCVD graphene syntheses. Interestingly, graphene syntheses using a Cu catalyst in APCVD processes at higher methane concentrations revealed that the growth is not self-limiting, which is in contrast to previous observations for the LPCVD case. Additionally, nanoribbons and nanostrips with widths ranging from 20 to 100 nm were also observed on the APCVD grown graphene. Interactions between graphene nanofeatures (edges, folds) and the contaminant metal nanoparticles from the Cu etchant were observed, suggesting that these samples could potentially be employed to investigate the chemical reactivity of single molecules, DNA, and nanoparticles with monolayer graphene.

KEYWORDS Graphene, CVD, kinetic models, copper, LPCVD, APCVD

Graphene, a single atomic layer of carbon atoms in a hexagonal network, has drawn significant attention with its unusual physical properties.[1−3] Proof-of-concept experiments demonstrating electronic and optoelectronic devices incorporating graphene as an active layer, such as high frequency transistors,[4,5] solar cells,[6−8] logic devices,[9] and interconnects in CMOS devices,[10] have been previously reported. To envision devices based on graphene, it is critical to synthesize large area graphene with high throughput and reliability. Recently, considerable research efforts focused on graphene synthesis using several different methods have succeeded in large area syntheses. Some of the most prominent methods that have enabled both small (μm^2) and large area (cm^2) syntheses of graphene include mechanical exfoliation,[11,12] chemical modification of graphene,[13−17] desorption of Si from either the Si plane or C plane of SiC substrates,[4,18,19] and catalyst-assisted synthesis in a chemical vapor deposition (CVD) process.[20−26] Mechanical exfoliation of graphene from bulk graphite has enabled fundamental investigations on the physical properties of graphene; however, using this technique it has not been possible yet to make large area graphene (wafer scale). Synthesis of graphene from SiC substrates has allowed larger area synthesis, and recently, field effect transistor devices fabricated from as-grown graphene have demonstrated unit gain frequencies up to 100 GHz.[4] Using metal-assisted thermal CVD for the synthesis of large areas of graphene is an exciting prospect for a number of reasons: (1) it allows large area graphene synthesis on a wafer scale with high uniformity and low defects, (2) it allows explororation of a wide variety of transition metals as catalysts and in elucidating the role of various process parameters, (3) it allows the integration with high volume CMOS-based technologies, and (4) it may enable an understanding the synthesis mechanism of graphene using metal catalysts.

Transition metal assisted CVD syntheses of graphene using different transition metals, including nickel, copper, ruthenium, and cobalt have been previously reported.[20−27] In these techniques, carbonaceous gaseous species are reacted at high temperatures (900−1100 °C) in the presence of metal thin films/foils, which serve both in the decomposition of the carbon species and in the nucleation of the graphene lattice. The mechanism of graphene growth on a metal catalyst is presumably influenced by factors, including the carbon solubility limit in the metal, its crystal structure, lattice parameter, and thermodynamic parameters such as the temperature and pressure of the system. By far, different growth mechanisms have been attributed primarily to the carbon solubility in the metal—in the case of very low carbon solubility catalysts (<0.001 atomic %) such as Cu, the synthesis of graphene is limited to the surface of the catalyst, and in the case of intermediate−high solubility (>0.1 atom %) metal catalysts, including Co and Ni, graphene synthesis is sug-

* To whom correspondence should be addressed, jingkong@mit.edu.
Received for review: 07/6/2010
Published on Web: 09/02/2010

DOI: 10.1021/nl102355e | *Nano Lett.* **2010,** *10,* 4128–4133

TABLE 1. Graphene Samples Synthesized at Various Gas Flow Compositions under APCVD and LPCVD Conditions Using a Cu Catalyst

	heating (H_2:Ar) in sccm	annealing (H_2:Ar) in sccm	growth (H_2:CH_4:Ar) in sccm	cooling (H_2:CH_4:Ar) in sccm
Cu APCVD-S1	200:0	200:0	200:18	200:18
Cu APCVD-S2	200:0	200:0	200:4.5	200:4.5
Cu APCVD-S3	50:450	50:450	50:2:450	50:2:450
Cu APCVD-S4	50:450	50:450	50:1:450	50:1:450
Cu APCVD-S5	50:450	50:450	50:450[a]	50:450[a]
Cu LPCVD-S6	10:0	10:0	7:15:0	7:15:0

[a] Note: The flow rate in this regime corresponded to 50 sccm of hydrogen gas along with 450 sccm of Ar containing 100 ppm methane.

gested to proceed via a combination of diffusion into the metal thin film at the growth temperature, and a precipitation of carbon from bulk to the surface of the metal upon cooling after CVD synthesis.[22−24]

Large area graphene synthesis using a Cu catalyst in a LPCVD process has received widespread attention since it was first reported in 2009.[22] This technique has provided researchers with a good method for the synthesis and fabrication of devices based on graphene. In this article, we demonstrate that the kinetics of graphene growth in a CVD process plays a critical role in the uniformity of large area graphene using a Cu catalyst. Although the thermodynamics of the synthesis system remains the same, whether the process is performed at atmospheric pressure, low pressure (LP) (0.1−1 Torr), or under ultrahigh vacuum (UHV) conditions (10^{-4}−10^{-6} Torr), the kinetics of the growth phenomenon are different, leading to a variation in the uniformity of the graphene over large areas (wafer scale). The kinetic models for atmospheric pressure CVD (APCVD) and low pressure CVD (LPCVD) are discussed, thereby providing insight for understanding the differences between APCVD vs LPCVD/UHVCVD.

APCVD Synthesis. Graphene syntheses under APCVD conditions were performed using two different gas mixtures (hydrogen and methane) and (hydrogen, argon, and methane). Copper foils (3 in. × 1 in.) were placed in an 1 in. quartz tube furnace and were heated to 1000 °C either in the presence of hydrogen gas alone or under a mixture of hydrogen and argon gas flow with varying compositions (see Table 1). Subsequently, methane gas was introduced in the furnace after the temperature stabilized and the syntheses were performed for 20−30 min. The samples were finally cooled to room temperature under hydrogen, methane, and argon gas flow.

LPCVD Synthesis. Graphene synthesis using Cu foil was performed according the time−temperature graph shown in supplementary Figure 1 in the Supporting information. The 3 in. × 1 in. Cu foils were placed in the furnace, and the growth chamber was pumped down to 10 mTorr using a vacuum pump. Hydrogen gas was introduced (total pressure 325 mtorr) into the system, and the Cu foils were heated to the growth temperature (1000 °C). The foils were annealed for 20−30 min to initiate Cu grain growth, remove residual copper oxide, and to smoothen the surface. Subsequently, methane gas was introduced (total pressure 625 mTorr, Table 1) in the chamber and the synthesis was performed for 30 min. The samples were cooled down under a flow of hydrogen and methane gas mixture.

Graphene Transfer from Copper to Different Substrates. Graphene growth is observed on two sides of the foil. The grown graphene on the Cu foils was cut into smaller samples (1 cm^2), and graphene on one side of the Cu foil was transferred on to a 300 nm SiO_2 substrate using the following method. First, a thin layer of poly(methyl methacrylate) (PMMA) (MicroChem 950 PMMA A9) diluted with anisole (1:1) was spin-cast on the as grown graphene on one side of the foil at 2500 rpm for a minute. Second, another layer of PMMA was spin-cast on top of the previous layer. The PMMA coated samples were baked at 130 °C for 5 min, and subsequently, oxygen plasma was used on the rear side of the Cu foil to remove the graphene. Copper was wet etched using a commercially available etchant (copper etchant Type CE-100, Transene Co.) for 30−60 min, resulting in graphene/PMMA films floating in the etchant. These films were then collected manually and first placed in deionized (DI) water for 10 min, followed by 10 min in 10% hydrochloric solution (except where mentioned otherwise), and finally in DI water before manually collecting them on to 300 nm SiO_2/Si substrates. Finally, PMMA was removed by annealing the samples at 450 °C for 90 min under hydrogen (700 sccm) and argon (300 sccm) gas flow.

Cu APCVD. The quality and the thickness uniformity of large area graphene were ascertained using optical microscopy from graphene that was transferred on to a silicon substrate with a 300 nm oxide layer. Optical micrographs of the transferred graphene on 300 nm SiO_2/Si substrates grown using Cu under atmospheric pressure CVD conditions and using different compositions of gases are shown in Figure 1 (also see Table 1). Graphene synthesized at higher methane concentrations (5−10% by volume, samples Cu APCVD S1-2) with hydrogen revealed that growth is nonuniform consisting of large multilayer domains with a monolayer background (Figure 1A−D). Interestingly, the shapes of multilayer domains varied based on the composition of the hydrogen in the total gas flow. These results also indicate that the graphene growth using a Cu catalyst is not self-limiting as has been previously observed in the case of LPCVD.[22] However, by lowering the methane concentrations in the gas mixture, the thickness uniformity was tailored to achieve a monolayer (Figure 1E−J). Monolayer graphene growth up to 96% of the total area was observed when methane gas with concentrations varying between 0.2% (by volume) and 100 ppm (ppm) were employed (sample Cu APCVD S5) (Figure 1 I,J).

Raman analysis of graphene was performed to ascertain the defect density, quality of the grown graphene, and the

DOI: 10.1021/nl102355e | Nano Lett. 2010, 10, 4128−4133

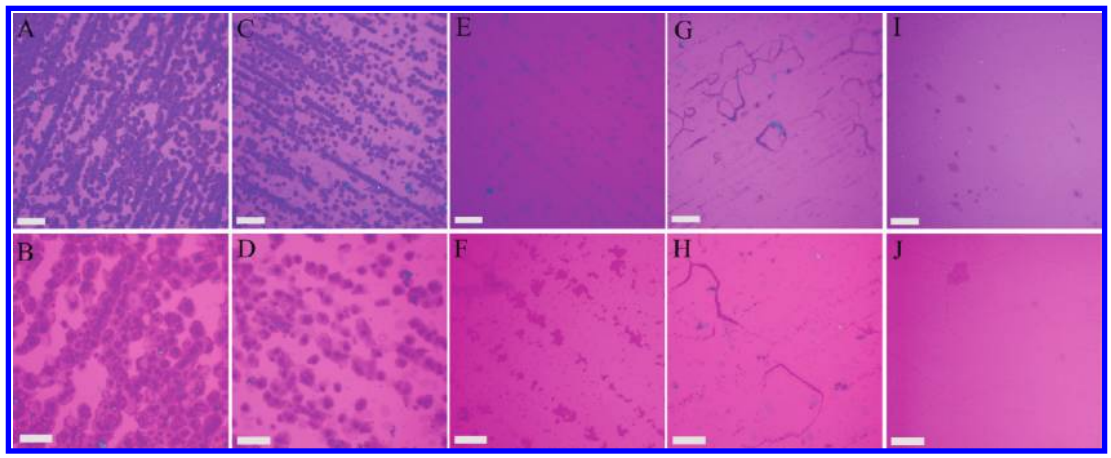

FIGURE 1. Optical images of transferred graphene on 300 nm SiO_2 synthesized under APCVD conditions using Cu as a catalyst at different methane gas compositions: S1 (A, B), S2 (C, D), S3 (E, F), S4 (G, H), and S5 (I, J); scale bars (A, C, E, G, I, 20 μm; B, D, F, H, J, 10 μm).

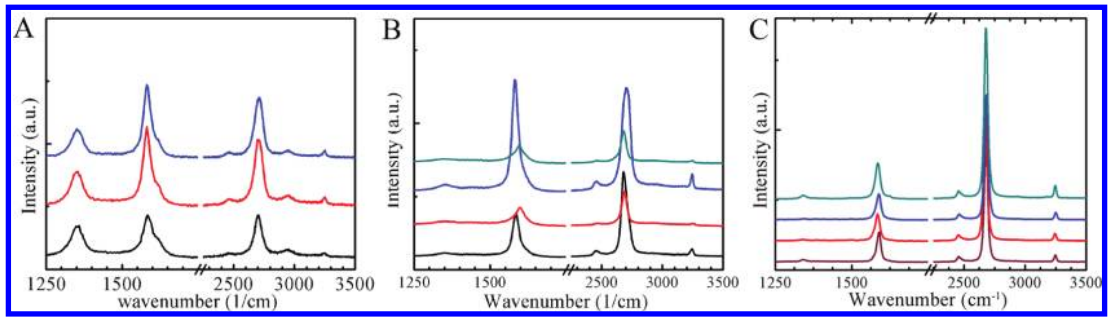

FIGURE 2. Raman spectra from transferred graphene on to 300 nm SiO_2 substrates synthesized using Cu as a catalyst under APCVD conditions. Multiple spectra from various spots from the same samples: (A) multilayer graphene domains from sample Cu APCVD S1; (B) multilayer domains (Cu APCVD S3); and (C) monolayer graphene (Cu APCVD S5).

variation in the thickness of the graphene films. Raman spectra were collected using a laser with an excitation wavelength of 532 nm and using an objective lens with 100 × magnification. Raman spectra collected from various multilayer domains from graphene synthesized at the highest methane concentration (sample Cu APCVD S1) and transferred to a 300 nm SiO_2 revealed a G′ peak with an average full width half maxima (fwhm) of more than 60 cm^{-1}, confirming the presence of multilayers in these domains (Figure 2A). The defect density was lower in the graphene samples synthesized at intermediate methane concentrations (Cu APCVD S3) (Figure 2B); however, there was variation in the D-band to G-band peak intensities from one location to another. The variation in the D to G peak intensities is unclear, and further evaluations are currently underway.

The Raman spectra from graphene synthesized at the lowest methane concentration (Cu APCVD S5) (Figure 2C) revealed a symmetric G′ peak with a FWHM of 35 cm^{-1} and the ratio of the peak intensities of the G′ peak to G peak was high (∼2−5) confirming the presence of monolayer graphene. The absence of D band intensity in these spectra also confirmed a higher quality of the as-grown graphene.

Transmission electron microscopy (TEM) of graphene was performed to determine its quality and to confirm the number of layers. TEM data were collected using either a JEOL 2010 or a JEOL 2010F instrument, operating at 200 kV. Graphene grown on copper foils was transferred to TEM grids (Quantifoil Cu 200 mesh) for performing these investigations. Representative high-resolution TEM images of transferred graphene grown are shown in Figure 3A,B. These data confirmed the presence of multilayer domains in the graphene samples synthesized at intermediate concentrations (Cu APCVD S3). Additionally, the number of layers in these multilayer domains varied between 2 and 5.

Transmission electron microscopy data collected from transferred graphene samples contaminated with copper etchant (containing iron) ions during the transfer process revealed new insights. The films in this case were not treated with a postcleaning step involving HCl solution after etching the Cu foil. Iron−iron oxide core−shell nanoparticles from the copper etchant decorated graphene edges and folds, indicating strong interactions between the edges/folds and the nanoparticles (Figure 3C). These nanoparticle decorated edges further enabled identification of nanosized features, revealing the presence of graphene nanoribbons and nanostrips with widths ranging from 20 to 100 nm in samples synthesized at intermediate methane concentrations (Figure 3D).

DOI: 10.1021/nl102355e | Nano Lett. 2010, 10, 4128–4133

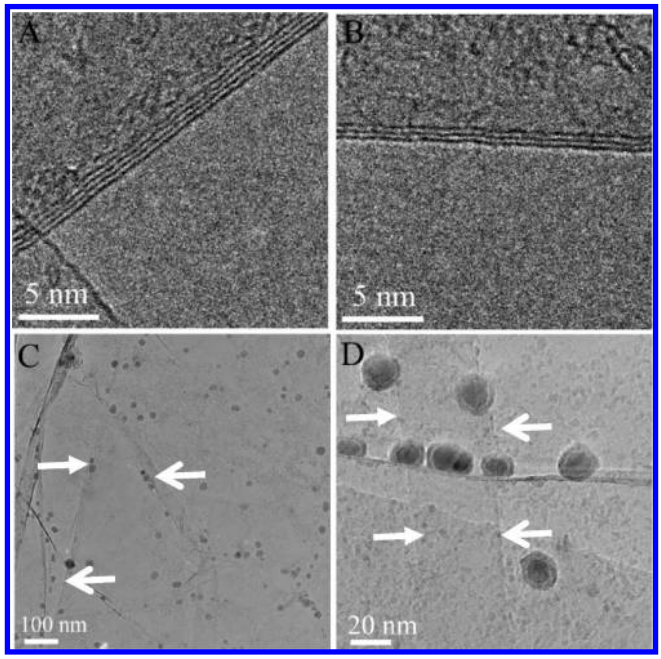

FIGURE 3. (A, B) High-resolution TEM images of graphene synthesized using Cu. (C) Contaminant nanoparticles (from the Cu etchant) decorating graphene edges/folds (indicated by arrows). (D) Graphene nanostrips and nanoribbons (along the arrows).

Thus, the Cu APCVD growth results varied from a monolayer at lower methane concentrations (parts per million concentration) to multilayer domains with a monolayer graphene background at higher methane concentrations (5−10% by volume), indicating that the growth is not self-limiting under higher methane concentrations. This result is different from previous observations in the case of a LPCVD process. Additionally, D-band intensities in the Raman spectra from APCVD samples were higher possibly due to higher methane gas flow rates, leading to gas reactions resulting in the deposition of particulates on the surface.

Cu LPCVD. Graphene synthesized using a Cu catalyst in a LPCVD process resulted in thickness uniformity across larger areas. This work was previously reported,[22] and independent investigations were performed here to draw a direct comparison between the APCVD and LPCVD processes in the same experimental setup. In accordance with previously reported data, our results also confirm the large area uniformity of as grown graphene. Representative characterization data of monolayer graphene synthesized using Cu at LPCVD are provided in the Supporting Information (supplementary Figure 2). The density of defects based on the absence of D peak intensity in the Raman spectra (supplementary Figure 2C in the Supporting Information) indicates a lower defect density compared to samples prepared under APCVD conditions (S1−S4). Differences in the kinetics process under LPCVD conditions are largely responsible for the thickness uniformity across large areas and lower defect density, and the pertinent analysis is provided in the next section.

Comparison of the Kinetic Processes between APCVD and LP/UHV CVD for Graphene Growth Using a Cu Catalyst. Thermodynamics of graphene synthesis using copper as a catalyst at a particular temperature in a CVD process is the same irrespective of whether the synthesis is performed under AP, LP, or UHV conditions. However, the kinetics of the processes are different. The kinetics (cooling rate, pressure of the reaction chamber during synthesis) of the CVD process has important ramifications on the growth rate of graphene films, thickness uniformity across large areas, and the density of defects. To emphasize the differences in the kinetics associated with the AP and LP/UHV CVD processes, we draw upon previously established CVD kinetic models[28−32] and modify them to account for synthesis of graphene using low carbon solid solubility catalysts. It is emphasized that the models we discuss here are applicable only to those catalysts which have very low carbon solubilities, resulting in diffusion of carbon either on the surface or limited to a few nanometers below the surface. Kinetic models for graphene synthesis using catalysts with intermediate to high carbon solid solubilities are currently being developed.

Figure 4A depicts a steady state gas flow of a mixture of methane, hydrogen, and argon gases on the surface of a Cu catalyst at a synthesis temperature (typically 1000 °C). We assume that the boundary layer due to steady state gas flow is stagnant and its thickness is δ. The carbon species first (1) diffuse through the boundary layer and reach the surface, and at the surface they get (2) adsorbed on the surface, (3) decompose to form active carbon species, (4) diffuse on the surface of the catalyst or into the catalyst close to the surface and form the graphene lattice, (5) inactive species (such as hydrogen) get desorbed from the surface, form molecular hydrogen, and (6) diffuse away from the surface through the boundary layer and are eventually swept away by the bulk gas flow. Depending upon whether the processes take place in the boundary layer (1, 6) or near or closer to the surface (2−4), they can be classified into two regimes: mass transport region, primarily involving diffusion through the boundary layer, and surface reaction region. Processes that take place on or close to the surface are largely affected by the temperature of the substrate. Over all, there are two fluxes of the active species that coexist: flux of active species through the boundary layer and the rate at which the active species are consumed at the surface of the catalyst to form the graphene lattice (Figure 4B). The equations for these fluxes are given by

$$F_{\text{mass transport}} = h_g(C_g - C_s) \quad (1)$$

$$F_{\text{surface reaction}} = K_s C_s \quad (2)$$

where, the $F_{\text{mass-transport}}$ is the flux of active species through the boundary layer, $F_{\text{surface-reaction}}$ is the flux of consumed

DOI: 10.1021/nl102355e | Nano Lett. 2010, 10, 4128–4133

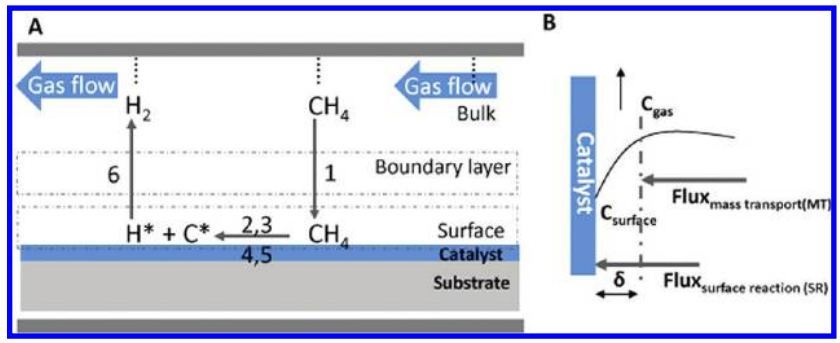

FIGURE 4. (A) Processes involved during graphene synthesis using low carbon solid solubility catalysts (Cu) in a CVD process. (B) Mass transport and surface reaction fluxes under steady state conditions.

active species at surface (assuming first-order kinetics), h_g is the mass transport coefficient, K_s is the surface reaction constant (assuming first-order rate kinetics), C_g is the concentration of gas in the bulk, and C_s is the concentration of the active species at the surface. These fluxes are in series, and the slower of the two processes is the rate-limiting step during graphene synthesis. At steady state, $F_{\text{mass-transport}} = F_{\text{surface-reaction}} = F_{\text{total-flux}}$, and the total flux ($F_{\text{total-flux}}$) after eliminating C_s can be rewritten as $[K_s h_g/(K_s + h_g)]C_g$. Mathematically, three regimes arise: $h_g \gg K_s$ (surface reaction controlled region), $h_g \sim K_s$ (mixed region), and $h_g \ll K_s$ (mass transport limited region). At high temperatures, under typical APCVD conditions, mass transport through the boundary layer is rate limiting ($K_s \gg h_g$), and under LP and UHV conditions, the surface reaction is the rate limiting step ($h_g \gg K_s$) (discussed below).

During CVD graphene synthesis under atmospheric conditions at higher syntheses temperatures (>900 °C), diffusion through the boundary layer is usually the rate limiting step ($K_s \gg h_g$) and the process is governed by this step (at higher temperatures surface reactions occur much faster due to the dependence on the Arrhenius term). This essentially translates to the fact that geometric effects of the gas flow and of the geometry of the CVD chamber play a critical role in the overall synthesis. A variation in the thickness of the boundary layer leads to a variation in the amount of active species that are diffusing through the boundary layer, resulting in the thickness nonuniformity of as grown graphene. During graphene synthesis in a batch process consisting of a stack of wafers, the boundary layers vary from wafer to wafer and also vary along the surface of the wafer (due to defects/dust) leading to thickness nonuniformities. In addition, the typical flow rates of active components under APCVD conditions are higher and can possibly lead to gas phase reactions in the bulk gas flow, depositing particulates on the surface of the graphene/catalyst resulting in a higher defect density. To avoid the deleterious boundary layer and the geometric effects on graphene synthesis, it is critical to perform the synthesis in the surface reaction regime, where the processes are primarily dependent on the temperature of the substrate. As long as the temperature across the wafer is maintained constant, graphene synthesis is expected to be uniform across the length of the wafer. Transitioning to the surface reaction limited regime at higher synthesis temperatures could be accomplished by lowering the pressure of the CVD chamber. At low pressures, the flux of active species is lower, leading to fewer collisions and a higher diffusitivity coefficient (D_g); $D_g \propto 1/(\text{total pressure})$. The mass transfer coefficient is related to the diffusion coefficient by the relation $h_g = D_g/\delta$ (see Supporting Information). At lower pressures, the boundary layer also increases, but the increase in D_g is significantly higher compared to an increase in the thickness of the boundary layer. The overall effect is that h_g increases as a result of lowering the total pressure and the diffusion through the boundary layer is enhanced, and it is no longer the rate limiting step under appropriate synthesis conditions ($h_g \gg K_s$). Under these conditions, the surface reaction regime is rate limiting, and as long as the temperature is maintained uniform across the length of the wafer and across the wafers, the thickness of the graphene is uniform.

In summary, graphene syntheses using Cu catalyst under APCVD conditions using a range of methane gas compositions revealed that growth varied from monolayer graphene at low methane concentrations (ppm) to multilayer domains on a monolayer at higher methane concentrations (5−10% by volume). Interestingly, these results reveal that graphene growth using Cu catalyst under APCVD conditions with higher methane concentration is not self-limiting as observed in the case of LPCVD, suggesting that further investigations have to be performed to determine the detail growth mechanism. The role of kinetic processes in graphene syntheses using low carbon solid solubility catalysts under APCVD and LPCVD conditions was elucidated.

Acknowledgment. This work was supported by the National Science Foundation under Award Number DMR 0845358, the MRSEC Program of the National Science Foundation under Award Number DMR 0819762, and the Graphene Approaches to Terahertz Electronics (GATE)—MURI Grant N000140911063 A00001.

Supporting Information Available. A schematic of the time−temperature curve providing details on LPCVD synthesis of graphene, a figure on the graphene characterization

DOI: 10.1021/nl102355e | *Nano Lett.* **2010,** *10,* 4128–4133

(optical micrograph, HR-TEM image and Raman spectra) synthesized using Cu catalyst under LPCVD conditions, and the derivation of relation $h_g = D_g/\delta$. This material is available free of charge via the Internet at http://pubs.acs.org.

REFERENCES AND NOTES

(1) Novoselov, K. S. A.; Geim, K.; Morozov, S. V.; Jiang, D.; Katsnelson, M. I.; Grigorieva, I. V.; Dubonos, S. V.; Firsov, A. A. *Nature* **2005**, *438*, 197–200.

(2) Morozov, S. V.; Novoselov, K. S.; Katsnelson, M. I.; Schedin, F.; Elias, D. C.; Jaszczak, J. A.; Geim, A. K. *Phys. Rev. Lett.* **2008**, *100*, No. 016602.

(3) Chen, J.-H.; Jang, C.; Xiao, S.; Ishigami, M.; Fuhrer, M. S. *Nat. Nanotechnol.* **2008**, *3*, 206–209.

(4) Lin, Y.-M.; Dimitrakopoulos, C.; Jenkins, K. A.; Farmer, D. B.; Chiu, H.-Y.; Grill, A.; Avouris, P. *Science* **2010**, *327*, 662.

(5) Lin, Y.-M.; Jenkins, K. A.; Valdes-Garcia, A.; Small, J. P.; Farmer, D. B.; Avouris, P. *Nano Lett.* **2009**, *9*, 422–426.

(6) Wang, X.; Zhi, L. J.; Mullen, K. *Nano Lett.* **2008**, *8* (1), 323–327.

(7) Wu, J. B.; Becerril, H. A.; Bao, Z. N.; Liu, Z. F.; Chen, Y. S.; Peumans, P. *Appl. Phys. Lett.* **2008**, *92* (26), 263302. Wang, Y.; Chen, X. H.; Zhong, Y. L.; Zhu, F. R.; Loh, K. P. *Appl. Phys. Lett.* **2009**, *95* (6), No. 063302.

(8) Li, X.; Zhu, Y.; Cai, W.; Borysiak, M.; Han, B.; Chen, D.; Piner, R. D.; Colombo, L.; Ruoff, R. S. *Nano Lett.* **2009**, *9* (12), 4359–4363.

(9) Sordan, R.; Traversi, F.; Russo, V. *Appl. Phys. Lett.* **2009**, *94*, No. 073305.

(10) Chen, X.; Lee, K.-J.; Akinwande, D.; Close, G.; Yasuda, S.; Paul, B.; Fujita, S.; Kong, J.; Wong, H.-S. P. *IEEE Int. Electron Devices Meet.* **2009**, Paper 23.6.

(11) Novoselov, K. S.; Jiang, D.; Schedin, F.; Booth, T. J.; Khotkevich, V. V.; Morozov, S. V.; Geim, A. K. *Proc. Natl. Acad. Sci. U.S.A.* **2005**, *102*, 10451–10453.

(12) Blake, P.; Brimicombe, P. D.; Nair, R. R.; Booth, T. J.; Jiang, D.; Schedin, F.; Ponomarenko, L. A.; Morozov, S. V.; Gleeson, H. F.; Hill, E. W.; Geim, A. K.; Novoselov, K. S. *Nano Lett.* **2008**, *8* (6), 1704–1708.

(13) Stankovich, S.; Dikin, D. A.; Piner, R. D.; Kohlhaas, K. A.; Kleinhammes, A. J.; Yuanyuan, W.; Yue, N.; SonBinh, T.; Ruoff, R. S. *Carbon* **2007**, *45*, 1558–1565.

(14) Eda, G.; Fanchini, G.; Chhowalla, M. *Nat. Nanotechnol.* **2008**, *3*, 270–274.

(15) Li, D.; Mueller, M. B.; Gilje, S; Kaner, R. B.; Wallace, G. G. *Nat. Nanotechnol.* **2008**, *3*, 101–105.

(16) Li, X.; Zhang, G.; Bai, X.; Sun, X.; Wang, X.; Wang, E.; Dai, H. *Nat. Nanotechnol.* **2008**, *3*, 538–542.

(17) Worsley, K. A.; Ramesh, P.; Mandal, S. K.; Niyogi, S.; Itkis, M. E.; Haddon, R. C. *Chem. Phys. Lett.* **2007**, *445*, 51–56.

(18) Berger, C.; Song, Z. M.; Li, T. B.; Li, X. B.; Ogbazghi, A. Y.; Feng, R.; Dai, Z. T.; Marchenkov, A. N.; Conrad, E. H.; First, P. N.; de Heer, W. A. *J. Phys. Chem. B* **2004**, *108*, 19912–19916.

(19) Berger, C.; Song, Z. M.; Li, X. B.; Wu, X. S.; Brown, N.; Naud, C.; Mayou, D.; Li, T. B.; Hass, J.; Marchenkov, A. N.; Conrad, E. H.; First, P. N.; de Heer, W. A. *Science* **2006**, *312*, 1191–1196.

(20) Pan, Y.; Shi, D. X.; Gao, H. J. *Chin. Phys.* **2007**, *16*, 3151–3153.

(21) Sutter, P. W.; Flege, J.-I.; Sutter, E. A. *Nat. Mater.* **2008**, *7*, 406–411.

(22) Li, X.; Cai, W.; An, J.; Kim, S.; Nah, J.; Yang, D.; Piner, R.; Velamakanni, A.; Jung, I.; Tutuc, E.; Banerjee, S. K.; Colombo, L.; Ruoff, R. S. *Science* **2009**, *324* (5932), 1312–1314.

(23) Kim, K. S.; Houk Jang, Y. Z.; Lee, S. Y.; Kim, J. M.; Kim, K. S.; Ahn, J.-H.; Kim, P.; Choi, J. Y; Hong, B. H. *Nature* **2009**, *457*, 706–710.

(24) Reina, A.; Jia, X.; Ho, J.; Nezich, D.; Son, H.; Bulovic, V.; Dresselhaus, M. S.; Kong, J. *Nano Lett.* **2009**, *9* (8), 3087.

(25) Reina, A.; Thiele, S.; Jia, X.; Bhaviripudi, S.; Dresselhaus, M. S.; Schaefer, J.; Kong, J. *Nano Res.* **2009**, *2*, 509–516.

(26) Yu, Q.; Lian, J.; Siriponglert, S.; Li, H.; Chen, Y. P.; Pei, S.-S. *Appl. Phys. Lett.* **2008**, *93* (11), 113103–113106.

(27) Vaari, J.; Lahtinen, J.; Hautojaŕvi, P. *Catal. Lett.* **1997**, *44* (1), 43–49.

(28) Joyce, B. A.; Bradley, R. R. *J. Electrochem. Soc.* **1963**, *110*, 1236–1240.

(29) Eversteyn, F. C.; Severin, P. J. W. *J. Electrochem. Soc.* **1970**, *117*, 925–931.

(30) Claassen, W. A. P.; Bloem, J. *Philips J. Res.* **1981**, *36*, 122–137.

(31) Kamins, T. *Polycrystalline Silicon for Integrated Circuit Applications*; Kluwer Academic Publishers: Norwell, MA, 1988; Chapter 1.

(32) Tao, M. *Thin Solid Films* **1993**, *223*, 201–211.

DOI: 10.1021/nl102355e | *Nano Lett.* **2010,** *10,* 4128–4133